Tuning Texture and Morphology of Mesoporous TiO2 by Non-Hydrolytic Sol-Gel Syntheses

Yanhui Wang, Maroua Bouchneb, Johan Alauzun, P. Hubert Mutin

molecules

MDPI

Article

Tuning Texture and Morphology of Mesoporous TiO_2 by Non-Hydrolytic Sol-Gel Syntheses

Yanhui Wang, Maroua Bouchneb, Johan G. Alauzun and P. Hubert Mutin *

Institut Charles Gerhardt, CNRS-UM-ENSCM, Université Montpellier, 34095 Montpellier, France; yanhui.wang@umontpellier.fr (Y.W.); maroua.bouchneb@etu.umontpellier.fr (M.B.); johan.alauzun@univ-montp2.fr (J.G.A.)

* Correspondence: hubert.mutin@umontpellier.fr; Tel.: +33-467-144-943

Academic Editors: Ahmad Mehdi and Sébastien Clément

Received: 22 October 2018; Accepted: 14 November 2018; Published: 17 November 2018

Abstract: The development of powerful synthetic methodologies is paramount in the design of advanced nanostructured materials. Owing to its remarkable properties and low cost, nanostructured TiO_2 is widely investigated for applications such as photocatalysis, energy conversion or energy storage. In this article we report the synthesis of mesoporous TiO_2 by three different non-hydrolytic sol-gel routes, and we investigate the influence of the synthetic route and of the presence and nature of the solvent on the structure, texture and morphology of the materials. The first route is the well-known ether route, based on the reaction of $TiCl_4$ with $^iPr_2O$. The second and third routes, which have not been previously described for the synthesis of mesoporous TiO_2, involve the reaction of $Ti(O^iPr)_4$ with stoichiometric amounts of acetophenone and benzoic anhydride, respectively. All materials are characterized by XRD, N_2 physisorption and SEM. By playing with the non-hydrolytic route used and the reaction conditions (presence of a solvent, nature of the solvent, calcination), it is possible to tune the morphology and texture of the TiO_2. Depending on the reaction conditions, a large variety of mesoporous TiO_2 nanostructures could be obtained, resulting from the spontaneous aggregation of TiO_2 nanoparticles, either rounded nanoparticles, platelets or nanorods. These nanoparticle networks exhibited a specific surface area up to 250 $m^2\ g^{-1}$ before calcination, or up to 110 $m^2\ g^{-1}$ after calcination.

Keywords: non-hydrolytic sol-gel; TiO_2; mesoporosity

1. Introduction

Owing to its outstanding properties, low toxicity and low cost, TiO_2 has been attracting tremendous attention for environmental and energy applications [1] such as photocatalysis [2–4], catalysis [5], water-splitting [6], sensing [7] and energy conversion and storage [8–11].

The development of powerful synthetic methods plays a pivotal role in the design of advanced materials and much research has been dedicated to the synthesis of TiO_2 nanomaterials. The sol-gel process is the most common method used to synthesize metal oxides. The conventional methods are based on hydrolysis and condensation but, following the pioneering work of Vioux's group [12,13], several alternative non-hydrolytic (or non-aqueous) sol-gel routes have been developed to avoid the disadvantages of hydrolytic sol-gel, such as high hydrolysis-condensation rates of metal alkoxides, low degree of condensation, and formation of poorly crystalline oxo-hydroxides [14–18]. Non-hydrolytic sol-gel (NHSG) is performed in an organic medium and involves organic oxygen-donors, such as ethers or alcohols, instead of water. NHSG has been established as a powerful methodology for the synthesis of mesoporous oxide or mixed oxide xerogels [19,20] and of crystalline metal oxide nanoparticles [18].

Several NHSG routes have been used to prepare TiO_2 nanomaterials, notably the alkoxide route and ether routes based on the reaction at 40–150 °C of a titanium halide precursor (typically $TiCl_4$) with a stoichiometric amount of a titanium alkoxide (usually $Ti(O^iPr)_4$ or an ether (usually diisopropylether) [13,21]. These so-called alkoxide and ether routes have been successfully used to prepare mesoporous TiO_2-based materials [22–24] and nanoparticles [25–28].

Alcohols (e.g., isopropanol, tert-butanol or benzyl alcohol) have also been used as oxygen donors [21,29,30]. In particular, the benzyl alcohol route, based on the reaction of various Ti precursors ($TiCl_4$, $Ti(O^iPr)_4$) with excess of benzyl alcohol acting as solvent, oxygen donor and surface ligand, has been extensively used to prepare TiO_2 nanoparticles in the absence of a capping agent [30–32].

The NHSG synthesis of TiO_2 by the reaction of $Ti(O^iPr)_4$ with acetic anhydride was also attempted, but this reaction was found to be quite slow, even at 140 °C, and catalysis by $TiCl_4$ was required [21]. Anatase nanoparticles were obtained by the reaction of $Ti(O^iPr)_4$ with various ketones (e.g., acetone, acetophenone) or aldehydes (e.g., butyraldehyde, benzaldehyde) [33,34].

The objective of this work is to compare the synthesis of mesoporous TiO_2 by three different NHSG routes, and we explore the influence of the synthetic route and of the presence and nature of the solvent on the structure, texture and morphology of the resulting nanomaterials. The first route is the ether route, based on the reaction of $TiCl_4$ with $^iPr_2O$; this route has been extensively used for the synthesis of TiO_2, but the synthesis in non-polar solvents such as toluene, squalane or cyclohexane has not been reported. The second and third routes, which have not been previously described for the synthesis of mesoporous TiO_2, involve the reaction of $Ti(O^iPr)_4$ with stoichiometric amounts of acetophenone and benzoic anhydride, respectively.

2. Results

2.1. Synthesis of TiO_2 Samples and Reactions Involved

The synthesis of the different TiO_2 samples is detailed in the 'Materials and Methods' part. In all cases the precursor was reacted with 2 equivalents of the oxygen donor under autogenous pressure in a Teflon lined stainless steel autoclave. The samples were labeled TiO_2-X-Y, where X corresponds to the oxygen donor (E, A and B stand for diisopropylether, acetophenone and benzoic anhydride, respectively) and Y corresponds to the solvent (NS, Tol, Squ and CH stand for no solvent, toluene, squalane, and cyclohexane, respectively), as shown in Table 1. The yields upon calcination are very high (>90%) for the samples prepared by the ether and acetophenone routes, indicating very high degrees of condensation. Conversely, the calcination yields are much lower for the samples prepared by the benzoic anhydride route (53–78%), pointing to significantly lower degrees of condensation.

Table 1. Reaction conditions for the synthesis of the different TiO_2 samples.

Sample	Precursor (amount)	O-donor [a]	Solvent	Temperature (time)	Calc. yield [b]/%
TiO_2-E-NS	$TiCl_4$ (12.5 mmol)	$^iPr_2O$	none	110 °C (72 h)	93
TiO_2-E-Tol	$TiCl_4$ (12.5 mmol)	$^iPr_2O$	toluene (5 mL)	110 °C (72 h)	94
TiO_2-E-Squ	$TiCl_4$ (12.5 mmol)	$^iPr_2O$	squalane (5 mL)	110 °C (72 h)	96
TiO_2-E-CH	$TiCl_4$ (12.5 mmol)	$^iPr_2O$	cyclohexane (5 mL)	110 °C (72 h)	93
TiO_2-A-NS	$Ti(O^iPr)_4$ (4.4 mmol)	$PhCOCH_3$	none	200 °C (12 h)	92
TiO_2-A-Tol	$Ti(O^iPr)_4$ (4.4 mmol)	$PhCOCH_3$	toluene (10 mL)	200 °C (12 h)	95
TiO_2-A-Squ	$Ti(O^iPr)_4$ (4.4 mmol)	$PhCOCH_3$	squalane (10 mL)	200 °C (12 h)	96
TiO_2-B-NS	$Ti(O^iPr)_4$ (4.4 mmol)	$(PhCO)_2O$	none	200 °C (12 h)	56
TiO_2-B-Tol	$Ti(O^iPr)_4$ (4.4 mmol)	$(PhCO)_2O$	toluene (10 mL)	200 °C (12 h)	53
TiO_2-B-Squ	$Ti(O^iPr)_4$ (4.4 mmol)	$(PhCO)_2O$	squalane (10 mL)	200 °C (12 h)	78

[a] 2 equivalents relative to the precursor; [b] calcination yield (500 °C, 5 h, in air).

The reactions likely involved in the NHSG routes used in this work are summarized in Scheme 1. The ether route based on the reaction of diisopropylether ($^iPr_2O$) and $TiCl_4$ is well documented; it involves an etherolysis (Equation (1)) and a condensation step (Equation (2)), with, in both cases,

elimination of isopropyl chloride [21]. The acetophenone route has been described previously for the synthesis of TiO_2 [33] and $BaTiO_3$ [35] nanoparticles, using acetophenone as a solvent and an O-donor. However, in the present case, a stoichiometric amount of acetophenone was used (2 equivalents relative to $Ti(O^iPr)_4$). According to Pazik et al., the main pathway could involve the elimination of the ketal compound $PhCMe(O^iPr)_2$ (Equations (3) and (4)). Benzoic anhydride has not been used previously to prepare metal oxides, but the mechanism should be similar to the one reported for acetic anhydride, with formation of the ester $PhCOO^iPr$ (Equations (5) and (6)) [21].

Ether route

$$Ti\text{-}Cl + {}^iPr_2O \longrightarrow Ti\text{-}O^iPr + {}^iPrCl \quad (1)$$

$$Ti\text{-}O^iPr + Ti\text{-}Cl \longrightarrow Ti\text{-}O\text{-}Ti + {}^iPrCl \quad (2)$$

Acetophenone route

$$Ti\text{-}O^iPr + PhCOMe \longrightarrow Ti\text{-}OCPhMeO^iPr \quad (3)$$

$$Ti\text{-}OCPhMeO^iPr + Ti\text{-}O^iPr \longrightarrow Ti\text{-}O\text{-}Ti + PhCMe(O^iPr)_2 \quad (4)$$

Benzoic anhydride route

$$Ti\text{-}O^iPr + (PhCO)_2O \longrightarrow Ti\text{-}OCOPh + PhCOO^iPr \quad (5)$$

$$Ti\text{-}O^iPr + Ti\text{-}OCOPh \longrightarrow Ti\text{-}O\text{-}Ti + PhCOO^iPr \quad (6)$$

Scheme 1. Proposed reaction schemes for the NHSG routes used in this work.

2.2. Structural and Textural Characterization of TiO_2 Samples

2.2.1. Powder X-Ray Diffraction (XRD)

The powder XRD patterns of the TiO_2 samples before and after calcination (5 h at 500 °C in air) are displayed in Figure 1. The only crystalline phase detected was the anatase phase (JCPDS 21-1272). All samples prepared by the ether or the acetophenone routes appeared well crystallized, even before calcination. Conversely, the samples prepared by the benzoic anhydride route were poorly crystallized before calcination (TiO_2-B-Squ or TiO_2-B-NS) or even amorphous to XRD (TiO_2-B-Tol).

The crystallite size, evaluated by the Scherrer equation for the (101) reflection, ranged from 7 to 13 nm for the non-calcined samples and from 9 to 28 nm after calcination (Table 2). The grain growth upon calcination was significant for the samples prepared by the ether route (e.g., from 9 to 23 nm for TiO_2-E-NS), while it was limited for the samples prepared by the acetophenone route (e.g., from 11 to 12 nm for TiO_2-A-NS).

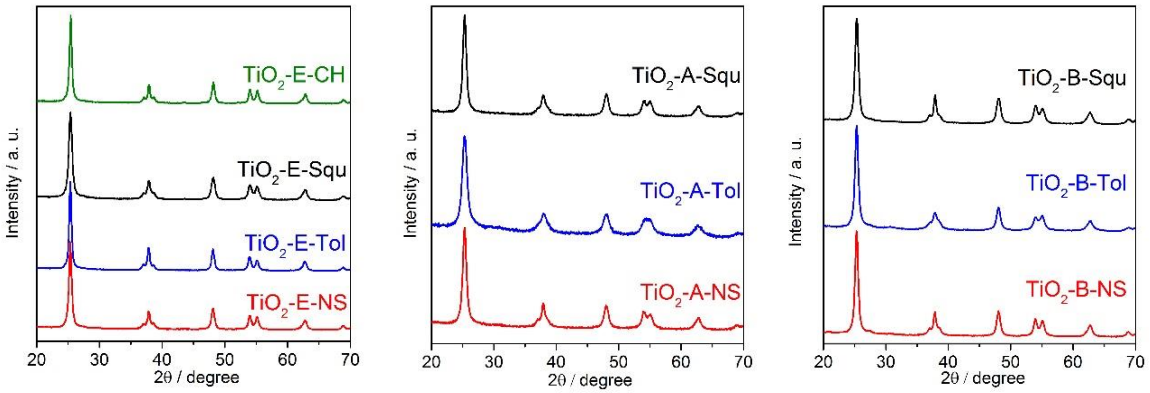

Figure 1. *Cont.*

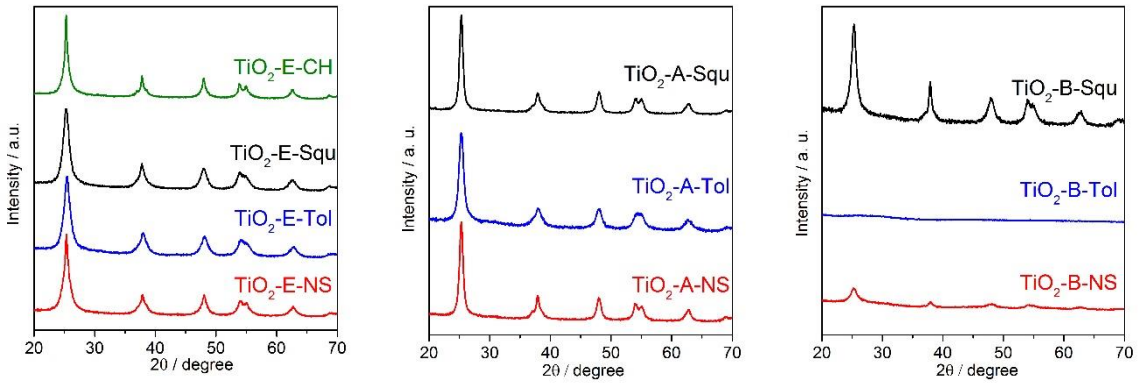

Figure 1. Powder X-ray diffraction (XRD) patterns of non-calcined (**bottom**) and calcined (**top**) TiO_2 samples.

Table 2. Crystallite size and textural data for the different TiO_2 samples, before and after calcination.

Sample	Calcination	Cryst. size [a] (nm)	S_{BET} [b] ($m^2\ g^{-1}$)	Vp [c] ($cm^3\ g^{-1}$)	Vmeso [d] ($cm^3\ g^{-1}$)	Dp [e] (nm)
TiO_2-E-NS	no	9	180	0.28	0.27	5
	yes	23	70	0.19	0.18	9
TiO_2-E-Tol	no	8	130	0.10	0.08	4
	yes	28	60	0.15	0.15	7
TiO_2-E-Squ	no	8	170	0.31	0.31	7
	yes	17	80	0.24	0.23	10
TiO_2-E-CH	no	13	130	0.18	0.17	5
	yes	28	50	0.14	0.14	9
TiO_2-A-NS	no	11	90	0.32	0.32	10
	yes	12	70	0.29	0.28	12
TiO_2-A-Tol	no	9	120	0.35	0.35	10
	yes	9	110	0.35	0.35	11
TiO_2-A-Squ	no	12	120	0.48	0.48	13
	yes	13	100	0.35	0.34	10
TiO_2-B-NS	no	9	240	0.13	0.02	3
	yes	12	80	0.15	0.15	6
TiO_2-B-Tol	no	am.	250	0.14	0.03	3
	yes	13	<10	<0.05	NA	NA
TiO_2-B-Squ	no	7	240	0.16	0.07	4
	yes	14	90	0.42	0.42	15

[a] crystallite size estimated by the Scherrer equation; [b] BET specific surface area; [c] total pore volume at $P/P_0 = 0.99$; [d] BJH volume of pores in the 2 to 50 nm range, calculated from the desorption branch. [e] BJH average mesopore diameter calculated from the desorption branch.

2.2.2. Nitrogen Physisorption

The texture of the TiO_2 samples before and after calcination was investigated using nitrogen physisorption at 77 K. Typical textural data (BET specific surface area, total pore volume and BJH average pore diameter) are displayed in Table 2. The adsorption−desorption isotherms and pore size distributions of the non-calcined and calcined samples are given in Figures 2 and 3, respectively.

Except for the calcined TiO_2-B-Tol sample, which is non porous, all the samples show significant specific surface areas ranging from 90 to 250 $m^2\ g^{-1}$ for the non-calcined samples and from 50 to 110 $m^2\ g^{-1}$ for the calcined ones.

According to the IUPAC classification [36], the isotherms of the calcined porous samples are either of type IVa (well-defined mesoporosity, e.g., calcined TiO_2-A-NS, TiO_2-A-Tol, TiO_2-A-Squ, TiO_2-B-NS) or are composite Type IVa + Type II isotherms (e.g., calcined TiO_2-E-NS, TiO_2-E-Tol, TiO_2-E-squ, TiO_2-E-CH), indicating the presence of both well-defined mesopores and macropores [36].

BJH analysis confirms the presence of mesopores with average diameters ranging from ca 3 to 30 nm, depending on the NHSG route used and on the solvent. The isotherms of the non-calcined samples (Figure 2) are similar to those of the calcined samples, with the exception of the samples prepared by the benzoic anhydride route which show type I or type I + IV isotherms, indicating the presence of micropores.

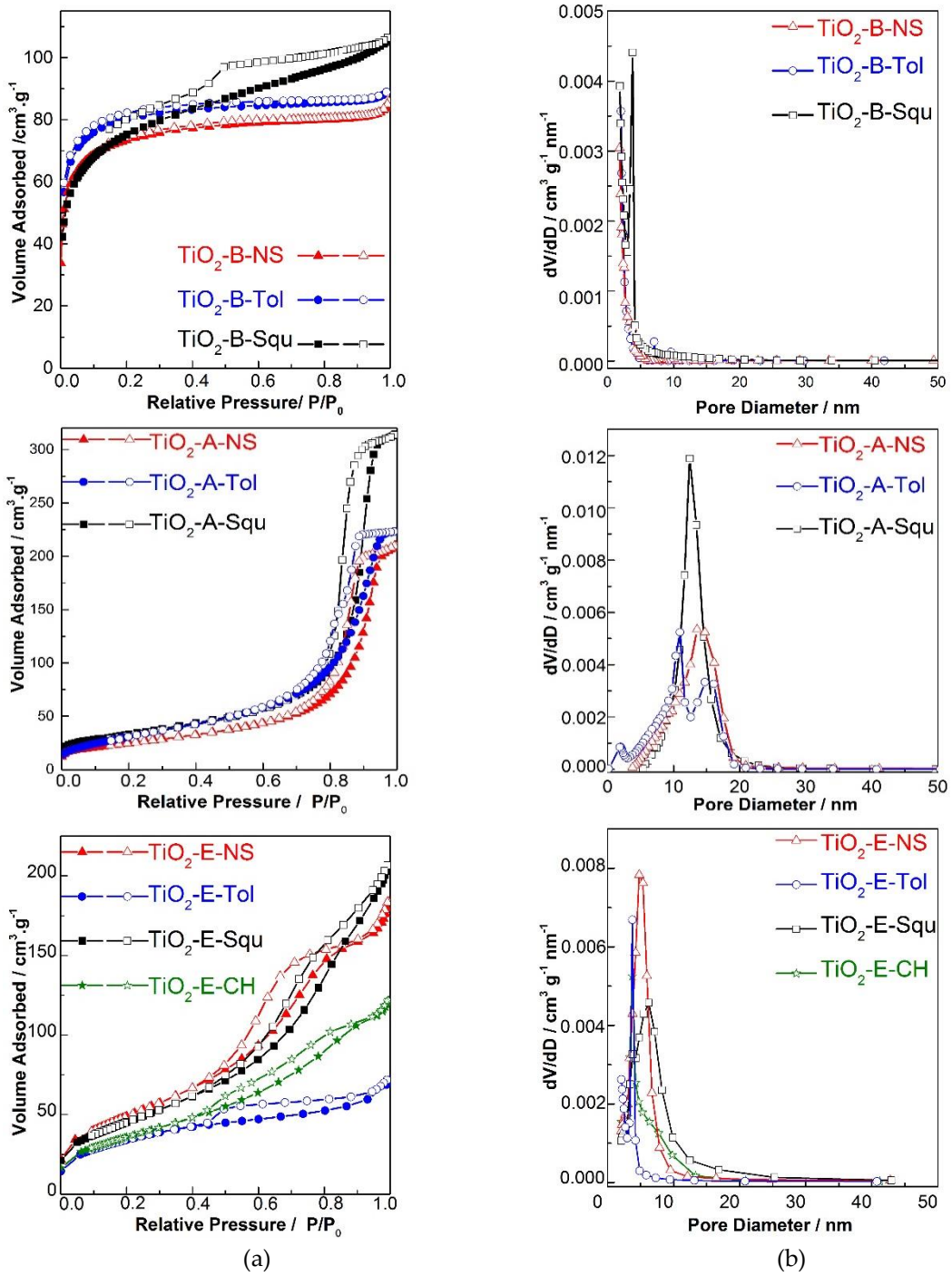

Figure 2. Nitrogen physisorption isotherms (**a**) and pore size distribution (**b**) of non-calcined TiO_2 samples. Filled and open symbols refer to adsorption and desorption, respectively.

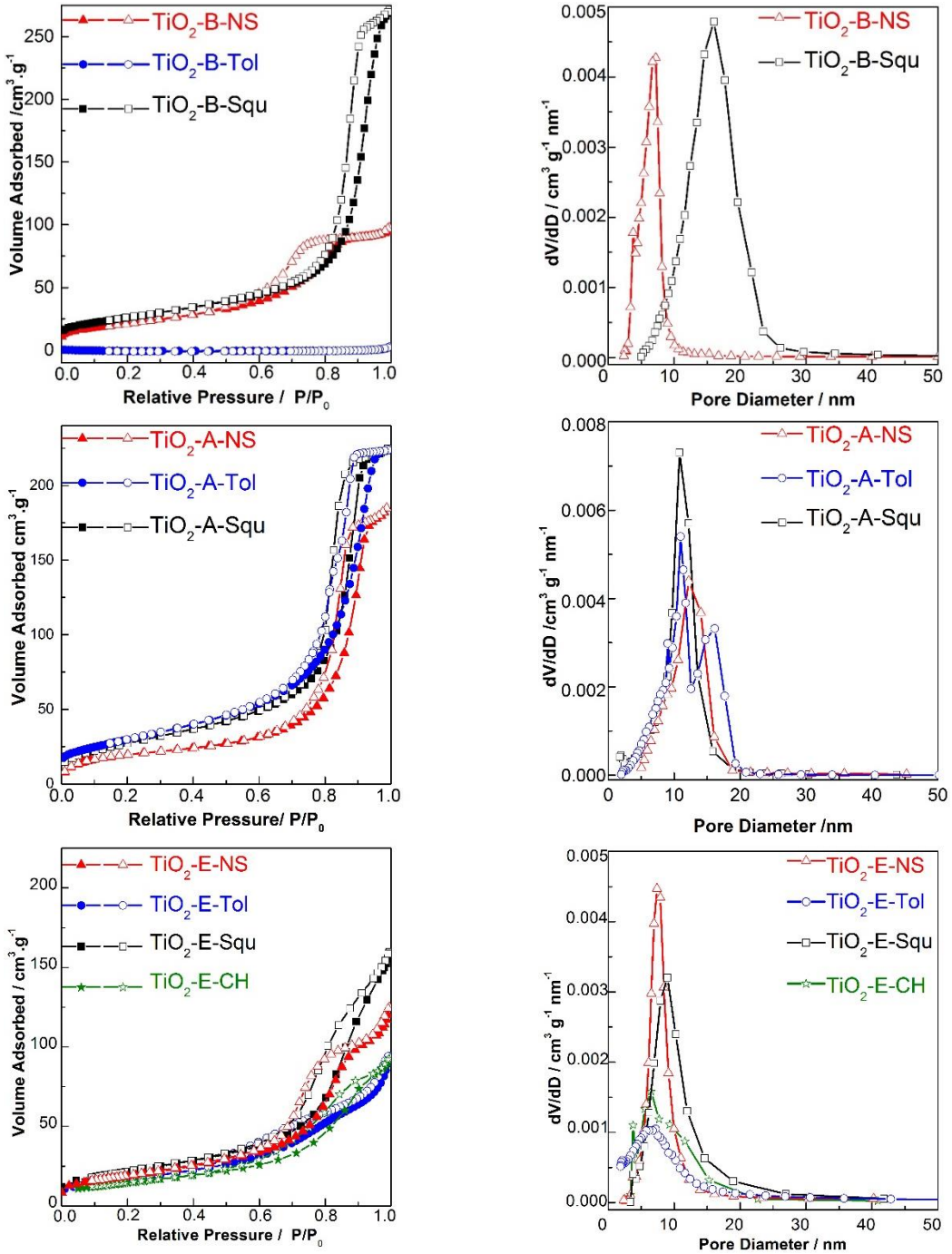

Figure 3. Nitrogen physisorption isotherms (**a**) and pore size distribution (**b**) of calcined TiO_2 samples. Filled and open symbols refer to adsorption and desorption, respectively.

2.3. Morphology of TiO_2 Samples

As shown in Figure 4, the morphology of the calcined samples depends both on the oxygen donors and the solvents used. The primary nanoparticles exhibit different morphologies and size. In most cases they are well-calibrated, roughly spherical nanoparticles with sizes ranging from ≈5 to 15 nm, but can be also platelets ≈50 nm in width and ≈10 nm thick (TiO_2-E-NS) or rods up to 1 μm in length (TiO_2-E-Tol). These primary nanoparticles either form large, more or less compact aggregates (e.g.,

TiO_2-E-Tol, TiO_2-A-NS, TiO_2-A-Tol, TiO_2-B-NS, TiO_2-B-Squ) or form spherical secondary aggregates, ≈1 to 15 μm in size (e.g., TiO_2-E-NS, TiO_2-E-Squ, TiO_2-E-CH, TiO_2-A-Squ, TiO_2-B-Tol).

In the case of the TiO_2-B-Tol sample, prior to calcination (Figure S1), the particles were very small but not sintered together, whereas after calcination (Figure 4) the sintered nanoparticles formed highly compact secondary aggregates, accounting for the negligible specific surface area and porosity of this sample.

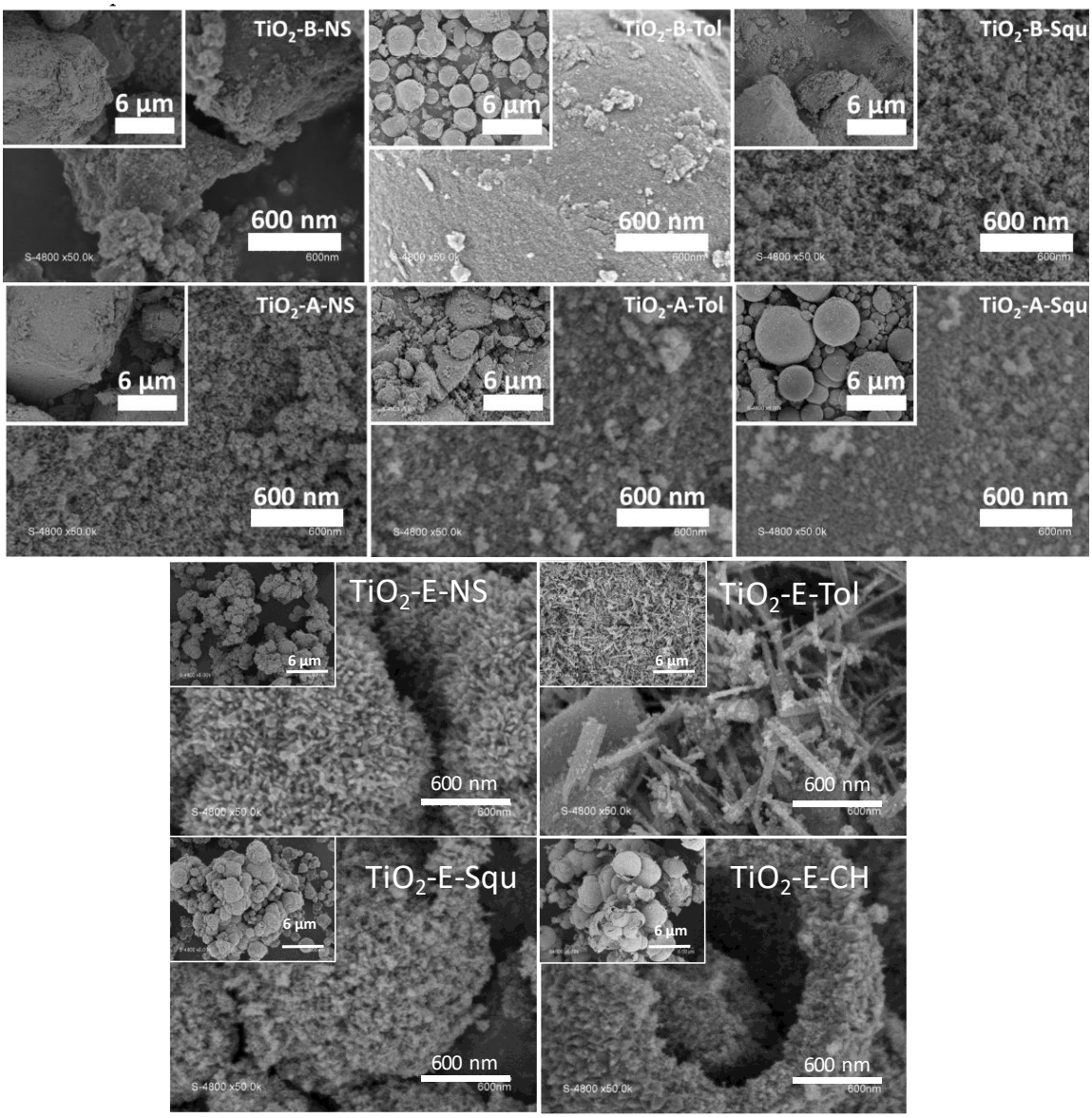

Figure 4. SEM images of calcined TiO_2 samples.

3. Discussion

The aim of this article was to investigate the influence of different NHSG routes and of the presence and nature of the solvent on the structure, texture and morphology of the materials. The first route is the well-known ether route, based on the reaction of $TiCl_4$ with $^{i}Pr_2O$. The second and third routes, which have not been previously described for the synthesis of mesoporous TiO_2, involve the reaction of $Ti(O^{i}Pr)_4$ with stoichiometric amounts of acetophenone and benzoic anhydride, respectively.

One important outcome of this work is that the acetophenone and benzoic anhydride routes offer efficient ways to obtain mesoporous TiO_2 materials, starting from the commercially available, easy to handle, $Ti(O^{i}Pr)_4$ precursor. For applications such as catalysis or sensing, the presence of

residual chloride groups may be a major drawback, thus avoiding the use of $TiCl_4$ as a precursor can be important. Additionally, the HCl released by the hydrolysis of chloride groups is highly corrosive.

In all three routes a stoichiometric amount of O-donor is used and solvent is not necessary, which from the point of view of atom economy is interesting. Nevertheless, playing with the route and reaction conditions offers simple and reproducible ways to tune the morphology and texture of the final TiO_2.

The calcination yields (Table 1) indicate very high degrees of condensation in the ether and acetophenone routes, and lower ones in the benzoic anhydride route. For instance, the ≈55% calcination yield of TiO_2-B-NS and TiO_2-B-Tol would correspond to a degree of condensation of ≈60% assuming an equal number of O^iPr and O(CO)Ph residual groups and complete conversion to TiO_2, as shown in Scheme 2.

$$TiO_{1.6}(OiPr)_{0.4}(OCOPh)_{0.4} \xrightarrow[air]{500\ ^\circ C} TiO_2 \qquad \Delta M/M0 = -45\%$$

Scheme 2. Theoretical weight loss for a TiO_2 xerogel with a degree of condensation of ≈60% (assuming an equal number of O^iPr and O(CO)Ph residual groups and complete conversion to TiO_2).

Whatever the route and the solvent used in the synthesis, the only crystalline phase found in the resulting TiO_2 samples is the anatase phase, which is the most commonly obtained TiO_2 polymorph in non-hydrolytic sol-gel synthesis (although formation of rutile and brookite has been reported in the reaction of $TiCl_4$ with some alcohols) [21]. The samples prepared by the benzoic anhydride route were poorly crystallized before calcination, particularly the TiO_2-B-Tol and TiO_2-B-NS samples. This behavior is quite uncommon, as NHSG syntheses are noted for yielding well-crystallized metal oxides even before calcination, and is likely related to the low degree of condensation of these xerogels.

The morphology of the calcined samples is very much dependent on the reaction conditions. The shape and size of the primary particles is more varied in the ether route (spheres, platelets or nanorods), whereas only spherical primary particles are observed in the other routes. Formation of micron-sized, spherical secondary particles is observed in all the routes (TiO_2-B-Tol, TiO_2-A-Squ, TiO_2-B-NS, TiO_2-E-Squ and TiO_2-E-CH), but there is no correlation with the nature of the solvent. Actually, it is well known in nanoparticle synthesis that both the morphology and arrangement of the crystallites can be tuned by the addition of small amounts of ligands. In our case, the different morphologies observed are likely governed by the nature of the residual groups and reaction by-products, which depends on the route, and also by the properties of the solvent. As previously noted for the non-hydrolytic benzyl alcohol route [15], this sensitivity to the reaction conditions offers the possibility to tune the morphology of the samples, but predicting the morphology is not yet possible.

The same applies to the texture of the TiO_2 samples: depending on the route used and on the reaction conditions, materials with a wide range of specific surface areas and pore sizes can be obtained.

The specific surface area of a network built of non-porous nanoparticles depends on the size and shape of the primary nanoparticles and on their degree of sintering. As a result, the texture is sensitive to the calcination treatment, which may lead to particle growth and sintering. In the case of samples prepared by the diisopropylether or benzoic anhydride routes (except TiO_2-B-Tol), calcination leads to a decrease of the specific surface area by a factor of 2 to 3; this decrease can be mostly ascribed to the significant increase in crystallite size taking place during the calcination. Similarly, the loss of specific surface area upon calcination is moderate (decrease by a factor of 1.2 to 1.4) for the samples prepared by the acetophenone route which show very limited grain growth. The geometric specific surface area of monodisperse spherical anatase particles (non sintered) is given by the relationship $S_{geom} = 6000/(\rho.D)$, where ρ is the specific gravity (in g cm^{-3}) and D the diameter (in nm). For example, for anatase (ρ = 3.9 g cm^{-3}), this relationship gives S_{geom} values ranging from 154 to 62 m^2 g^{-1} for particle diameters ranging from 10 to 25 nm. In most cases, the specific surface area of the calcined samples is 5 to 40% lower than the geometric surface area estimated from their

crystallite size (from XRD data), indicating low to moderate sintering. The behavior of the sample TiO_2-B-Tol is outstanding. Prior to calcination, this sample was amorphous and exhibited a very high specific surface area (250 $m^2\ g^{-1}$); after calcination, the specific surface area decreased to less than 10 $m^2\ g^{-1}$, although the anatase nanocrystals formed were quite small (13 nm). This indicates complete sintering of the particles growing from an amorphous phase.

4. Materials and Methods

All manipulations were carried out under an argon atmosphere in a glovebox (<10 ppm H_2O and O_2). Titanium (IV) chloride ($TiCl_4$ 99%), titanium (IV) isopropoxide ($Ti(O^iPr)_4$ 97%), acetic anhydride (Ac_2O, 99%) and acetophenone (99%) were obtained from Sigma-Aldrich (St.Quentin Fallavier, France). Squalane (98%) was purchased from Alfa Aesar (Karlsruhe, Germany). Diisopropylether ($^iPr_2O$) and toluene (Sigma-Aldrich 99.7%) were dried over a Pure Solve MD5 solvent purification system (H_2O < 10 ppm). Cyclohexane (Sigma-Aldrich 99.5%) was dried over molecular sieves. All other chemicals were used without further purification.

TiO_2 samples were prepared without solvent or in the presence of a solvent (toluene, squalane or cyclohexane). The precursor ($TiCl_4$ or $Ti(O^iPr)_4$), the oxygen donor (2 equivalents relative to the precursor) and the solvent (if any) were mixed in a stainless steel digestion vessel equipped with a PTFE lining (23 mL). Then the sealed autoclave was heated in an oven under autogenous pressure. The reaction conditions are summarized in Table 1. After reaction, the resulting white precipitate was thoroughly washed with CH_2Cl_2 (Carlo Erba 99.8%) (TiO_2-E samples) or acetone (TiO_2-A and TiO_2-B samples). The precipitate was then dried under vacuum at room temperature for 5 h and then ground into a fine white powder. Calcination was carried out in a muffle furnace at 500 °C (heating rate 5 °C/min) for 5 h in ambient air.

X-Ray diffraction (XRD) patterns were recorded with $Cu_{K\alpha}$ radiation (λ = 1.5418 Å) on a PANalytical X'Pert Pro MPD diffractometer (Royston, United Kingdom). Crystallite size was estimated from the most intense reflection (25.28° 2θ) using the Scherrer equation. Scanning electron microscopy images were obtained with a Hitachi S-4800 electron microscope. N_2-physisorption experiments were performed at −196 °C on a Micromeritics TriStar 3000 (Merignac, France). The samples were de-gassed under vacuum at 180 °C for 15 h prior to measurement. The total pore volume was measured at P/P_0 > 0.985. The pore size distribution was derived by the BJH method from the desorption branch.

5. Conclusions

A set of ten TiO_2 samples was prepared by three different non-hydrolytic sol-gel routes, and the influence of the reaction conditions (presence of a solvent, nature of the solvent, calcination) on the structure, texture and morphology of the samples was investigated. The acetophenone route appears to be a promising, chloride-free, non-hydrolytic sol-gel route, giving well-crystallized anatase materials even before calcination and with very interesting mesoporous textures compared to the well-known ether route. The benzoic anhydride route appears less promising due to the low crystallinity and significant microporosity of the non-calcined samples and the dramatic loss of specific surface area upon calcination. In each route, playing with the presence and nature of the solvent offers the possibility to tune the morphology of the samples, but prediction is not yet possible.

Supplementary Materials: The following are available online. Figure S1: SEM images of non-calcined TiO_2 samples.

Author Contributions: All authors have contributed substantially to the work reported. Investigation, M.B., Y.W.; Writing-Original Draft Preparation, P.H.M.; Supervision, P.H.M., J.G.A.; Funding Acquisition, P.H.M., J.G.A.

Funding: This research was funded by the "Agence Nationale de la Recherche" grant numbers ANR-16-CE07-0010 and ANR-16-CE08-0015.

Acknowledgments: The authors thank the Centre National de la Recherche Scientifique (CNRS) and the Université de Montpellier for financial support.

Conflicts of Interest: The authors declare no conflicts of interest.

References

1. Chen, X.; Mao, S.S. Titanium Dioxide Nanomaterials: Synthesis, Properties, Modifications, and Applications. *Chem. Rev.* **2007**, *107*, 2891–2959. [CrossRef] [PubMed]
2. Lee, S.M.; Park, G.C.; Seo, T.Y.; Jung, S.-B.; Lee, J.H.; Kim, Y.D.; Choi, D.H.; Lim, J.H.; Joo, J. Facet-controlled anatase TiO_2 nanoparticles through various fluorine sources for superior photocatalytic activity. *Nanotechnology* **2016**, *27*, 395604. [CrossRef] [PubMed]
3. Nasr, M.; Eid, C.; Habchi, R.; Miele, P.; Bechelany, M. Recent Progress on Titanium Dioxide Nanomaterials for Photocatalytic Applications. *ChemSusChem* **2018**, *11*, 3023–3047. [CrossRef] [PubMed]
4. Ma, Y.; Wang, X.; Jia, Y.; Chen, X.; Han, H.; Li, C. Titanium dioxide-based nanomaterials for photocatalytic fuel generations. *Chem. Rev.* **2014**, *114*, 9987–10043. [CrossRef] [PubMed]
5. Oi, L.E.; Choo, M.-Y.; Lee, H.V.; Ong, H.C.; Abd Hamid, S.B.; Juan, J.C. Recent advances of titanium dioxide (TiO_2) for green organic synthesis. *RSC Adv.* **2016**, *6*, 108741–108754. [CrossRef]
6. Osterloh, F.E. Inorganic materials as catalysts for photochemical splitting of water. *Chem. Mater.* **2008**, *20*, 35–54. [CrossRef]
7. Bai, J.; Zhou, B. Titanium Dioxide Nanomaterials for Sensor Applications. *Chem. Rev.* **2014**, *114*, 10131–10176. [CrossRef] [PubMed]
8. Bai, Y.; Mora-Seró, I.; De Angelis, F.; Bisquert, J.; Wang, P. Titanium dioxide nanomaterials for photovoltaic applications. *Chem. Rev.* **2014**, *114*, 10095–10130. [CrossRef] [PubMed]
9. Weng, Z.; Guo, H.; Liu, X.; Wu, S.; Yeung, K.W.K.; Chu, P.K. Nanostructured TiO_2 for energy conversion and storage. *RSC Adv.* **2013**, *3*, 24758–24775. [CrossRef]
10. Fröschl, T.; Hörmann, U.; Kubiak, P.; Kučerová, G.; Pfanzelt, M.; Weiss, C.K.; Behm, R.J.; Hüsing, N.; Kaiser, U.; Landfester, K.; Wohlfahrt-Mehrens, M. High surface area crystalline titanium dioxide: Potential and limits in electrochemical energy storage and catalysis. *Chem. Soc. Rev.* **2012**, *41*, 5313. [CrossRef] [PubMed]
11. Song, T.; Paik, U. TiO_2 as an active or supplemental material for lithium batteries. *J. Mater. Chem. A* **2016**, *4*, 14–31. [CrossRef]
12. Corriu, R.J.P.; Leclercq, D.; Lefèvre, P.; Mutin, P.H.; Vioux, A. Preparation of monolithic binary oxide gels by a non-hydrolytic sol-gel process. *Chem. Mater.* **1992**, *4*, 961–963. [CrossRef]
13. Corriu, R.J.P.; Leclercq, D.; Lefèvre, P.; Mutin, P.H.; Vioux, A. Preparation of monolithic metal oxide gels by a non-hydrolytic sol–gel process. *J. Mater. Chem.* **1992**, *2*, 673–674. [CrossRef]
14. Vioux, A. Nonhydrolytic Sol−Gel Routes to Oxides. *Chem. Mater.* **1997**, *9*, 2292–2299. [CrossRef]
15. Pinna, N.; Niederberger, M. Surfactant-Free Nonaqueous Synthesis of Metal Oxide Nanostructures. *Angew. Chem. Int. Ed.* **2008**, *47*, 5292–5304. [CrossRef] [PubMed]
16. Mutin, P.H.; Vioux, A. Nonhydrolytic processing of oxide-based materials: Simple routes to control homogeneity, morphology, and nanostructure. *Chem. Mater.* **2009**, *21*, 582–596. [CrossRef]
17. Styskalik, A.; Skoda, D.; Barnes, C.; Pinkas, J. The Power of Non-Hydrolytic Sol-Gel Chemistry: A Review. *Catalysts* **2017**, *7*, 168. [CrossRef]
18. Deshmukh, R.; Niederberger, M. Mechanistic Aspects in the Formation, Growth and Surface Functionalization of Metal Oxide Nanoparticles in Organic Solvents. *Chem.-Eur. J.* **2017**, *23*, 8542–8570. [CrossRef] [PubMed]
19. Debecker, D.P.; Hulea, V.; Mutin, P.H. Mesoporous mixed oxide catalysts via non-hydrolytic sol–gel: A review. *Appl. Catal. A* **2013**, *451*, 192–206. [CrossRef]
20. Mutin, P.H.; Vioux, A. Recent advances in the synthesis of inorganic materials via non-hydrolytic condensation and related low-temperature routes. *J. Mater. Chem. Coruña* **2013**, *1*, 11504. [CrossRef]
21. Arnal, P.; Corriu, R.J.P.; Leclercq, D.; Mutin, P.H.; Vioux, A. Preparation of anatase, brookite and rutile at low temperature by non-hydrolytic sol–gel methods. *J. Mater. Chem.* **1996**, *6*, 1925–1932. [CrossRef]
22. Popa, A.F.; Mutin, P.H.; Vioux, A.; Delahay, G.; Coq, B. Novel non-hydrolytic synthesis of a V_2O_5–TiO_2 xerogel for the selective catalytic reduction of No_x by ammonia. *Chem. Commun.* **2004**, 2214–2215. [CrossRef] [PubMed]

23. Debecker, D.P.; Bouchmella, K.; Delaigle, R.; Eloy, P.; Poleunis, C.; Bertrand, P.; Gaigneaux, E.M.; Mutin, P.H. One-step non-hydrolytic sol–gel preparation of efficient V_2O_5-TiO_2 catalysts for VOC total oxidation. *Appl. Catal. B Environ.* **2010**, *94*, 38–45. [CrossRef]
24. Escamilla-Pérez, A.M.; Louvain, N.; Boury, B.; Brun, N.; Mutin, H. Ethers as oxygen donor and carbon source in non-hydrolytic sol-gel: One-pot, atom-economic synthesis of mesoporous TiO_2-carbon nanocomposites. *Chem. Eur. J.* **2018**, *24*, 4982–4990. [CrossRef] [PubMed]
25. Trentler, T.J.; Denler, T.E.; Bertone, J.F.; Agrawal, A.; Colvin, V.L. Synthesis of TiO_2 Nanocrystals by Nonhydrolytic Solution-Based Reactions. *J. Am. Chem. Soc.* **1999**, *121*, 1613–1614. [CrossRef]
26. Jun, Y.W.; Casula, M.F.; Sim, J.-H.; Kim, S.Y.; Cheon, J.; Alivisatos, A.P. Surfactant-Assisted Elimination of a High Energy Facet as a Means of Controlling the Shapes of TiO_2 Nanocrystals. *J. Am. Chem. Soc.* **2003**, *125*, 15981–15985. [CrossRef] [PubMed]
27. Koo, B.; Park, J.; Kim, Y.; Choi, S.-H.; Sung, Y.-E.; Hyeon, T. Simultaneous phase- and size-controlled synthesis of TiO_2 nanorods via non-hydrolytic sol−gel reaction of syringe pump delivered precursors. *J. Phys. Chem. B* **2006**, *110*, 24318–24323. [CrossRef] [PubMed]
28. Aboulaich, A.; Boury, B.; Mutin, P.H. Reactive and organosoluble anatase nanoparticles by a surfactant-free nonhydrolytic synthesis. *Chem. Mater.* **2010**, *22*, 4519–4521. [CrossRef]
29. Lou, F.; Qian, X.; Jin, Y.; Zhou, M. Characterisation of water-soluble TiO_2 and its photocatalytic activity under visible light. *Mater. Res. Innov.* **2015**, *19*, S8-693–S8-696. [CrossRef]
30. Niederberger, M.; Bartl, M.H.; Stucky, G.D. Benzyl alcohol and titanium tetrachloridea versatile reaction system for the nonaqueous and low-temperature preparation of crystalline and luminescent titania nanoparticles. *Chem. Mater.* **2002**, *14*, 4364–4370. [CrossRef]
31. Garnweitner, G.; Niederberger, M. Nonaqueous and Surfactant-Free Synthesis Routes to Metal Oxide Nanoparticles. *J. Am. Ceram. Soc.* **2006**, *89*, 1801–1808. [CrossRef]
32. Pinna, N.; Karmaoui, M.; Willinger, M.-G. The "benzyl alcohol route": An elegant approach towards doped and multimetal oxide nanocrystals. *J. Sol-Gel Sci. Technol.* **2011**, *57*, 323–329. [CrossRef]
33. Garnweitner, G.; Antonietti, M.; Niederberger, M. Nonaqueous synthesis of crystalline anatase nanoparticles in simple ketones and aldehydes as oxygen-supplying agents. *Chem. Commun.* **2005**, 397. [CrossRef] [PubMed]
34. Wu, Y.; Liu, H.-M.; Xu, B.-Q. Solvothermal synthesis of TiO_2: Anatase nanocrystals and rutile nanofibres from ticl4 in acetone. *Appl. Organomet. Chem.* **2007**, *21*, 146–149. [CrossRef]
35. Pazik, R.; Tekoriute, R.; Håkansson, S.; Wiglusz, R.; Strek, W.; Seisenbaeva, G.A.; Gun'ko, Y.K.; Kessler, V.G. Precursor and solvent effects in the nonhydrolytic synthesis of complex oxide nanoparticles for bioimaging applications by the ether elimination (bradley) reaction. *Chem.-Eur. J.* **2009**, *15*, 6820–6826. [CrossRef] [PubMed]
36. Thommes, M.; Kaneko, K.; Neimark, A.V.; Olivier, J.P.; Rodriguez-Reinoso, F.; Rouquerol, J.; Sing, K.S.W. Physisorption of gases, with special reference to the evaluation of surface area and pore size distribution (IUPAC technical report). *Pure Appl. Chem.* **2015**, *87*. [CrossRef]

Sample Availability: Samples of the compounds are not available from the authors.